

Effect of Collision Axes Offset of the Plasmoid in the Collisional Merging Process of FRC Plasma^{*)}

Hiroki SOMEYA, Tomohiko ASAI, Daichi KOBAYASHI, Taichi SEKI, Takuto YAMANAKA, Tatsuhiro WATANABE, Tsutomu TAKAHASHI and Naoki MIZUGUCHI¹⁾

College of Science and Technology, Nihon University, Tokyo 101-8308, Japan

¹⁾*National Institute for Fusion Science, Toki 509-5292, Japan*

(Received 10 January 2022 / Accepted 5 April 2022)

In this study, the effect of the collision axes offset in the collisional merging process of field-reversed configuration (FRC) in the FAT-CM (FRC amplification via translation-collisional merging) device was experimentally investigated for the first time. The offset of incident axes during collision does not exhibit any considerable effect on particle inventory and trapped magnetic flux of the merged FRC, which is inconsistent with the results predicted via the three-dimensional magnetohydrodynamic (MHD) simulation using the MHD infrastructure for plasma simulation (MIPS) code. Based on the obtained results, the FRC exhibits robust stability and it does not collapse even when subjected to destructive perturbations during the dynamic translation and collision processes.

© 2022 The Japan Society of Plasma Science and Nuclear Fusion Research

Keywords: field-reversed configuration, three-dimensional magnetohydrodynamic simulation, offset

DOI: 10.1585/pfr.17.2402068

1. Introduction

A field-reversed configuration (FRC) is a magnetic confinement system classified as a compact torus. An FRC is considered a high-beta system because its volume-averaged beta value is approximately unity ($\langle\beta\rangle \sim 1$), which is the highest among the toroidal magnetic confinement systems [1, 2].

The collisional merging formation of an FRC has been attempted in the FRC amplification via a translational-collisional merging (FAT-CM) device at the Nihon Uni-

versity [3]. During the formation process, the two initial FRC-like plasmoids, which were formed using a conical field-reversed theta pinch method, are accelerated up to supersonic/Alfvénic speed using a magnetic pressure gradient toward the device axis [4] and they collide and merge into a single FRC plasma near the midplane (Fig. 1). The two initial plasmoids are said to be FRC-like because they have an FRC-like reversed magnetic structure with a small toroidal field component. However, an FRC is unstable in the radial direction and causes internal/external tilt and

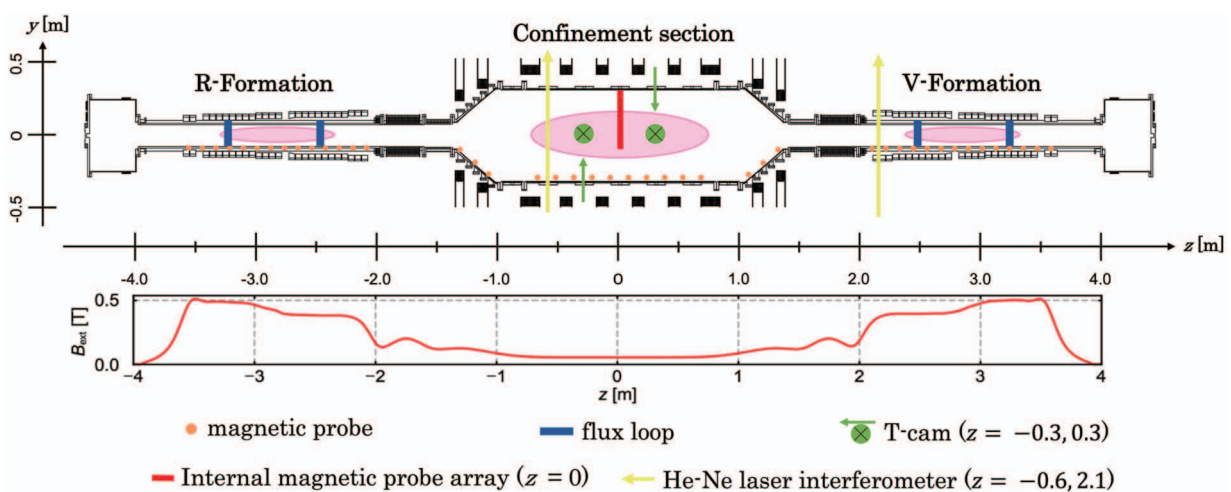


Fig. 1 Schematic of the FAT-CM device and the axial profile of the external guide magnetic field.

author's e-mail: asai.tomohiko@nihon-u.ac.jp

^{*)} This article is based on the presentation at the 30th International Toki Conference on Plasma and Fusion Research (ITC30).

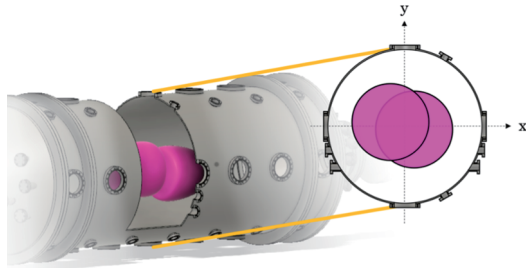


Fig. 2 Image of the offset collision.

wobble motion because of its simply connected geometry. During the translation process, the FRC may move in a radial direction. Therefore, there is a high possibility that the head-on collision of the two initial plasmoids does not occur. We hypothesized that the offset of the translational axes of plasmoids during the collision would affect the FRC performance after the collision/merging formation.

In this study, we experimentally investigated the effect of the offset of the plasmoid's collision axes using particle inventory and trapped magnetic flux as indicators. Herein, the offset of the plasmoid's collision axes describes the distance of the radial shift from the axes of translation of the two initial plasmoids (Fig. 2). Furthermore, we evaluate the dependence of the particle loss during the collisional merging process and the poloidal magnetic flux of the merged FRC on the offset of the plasmoid's collision axes via the simultaneous multipointed density measurements and the internal magnetic probe array [5]. In addition, the three-dimensional (3D) simulation using the magnetohydrodynamic (MHD) infrastructure for plasma simulation (MIPS) code was used to simulate the asymmetric collision/merging process of FRC in [6].

2. Experimental Setup

Figure 1 shows that the FAT-CM device is symmetrical with the midplane ($z = 0$) of the device and comprises two formation sections (V- and R-formations) and a confinement section. Figure 1 shows the axial profile of the external guide magnetic field. The FRC plasma radius can be estimated by the excluded flux measurement using a magnetic probe and flux loop [7]. If the curvature of the FRC plasma edge is negligible, the excluded flux radius is comparable to the separatrix radius. For estimating the excluded flux radius, at each formation section, 14 magnetic probes were placed at intervals of 0.11 m and two flux loops were installed. In the confinement section, 16 magnetic probes placed at intervals of 0.15 m were installed along the chamber wall. The excluded flux radius $r_{\Delta\phi}$ is calculated as follows:

$$r_{\Delta\phi} = r_w \sqrt{1 - \frac{\phi_p B_v}{\phi_v B_p}}, \quad (1)$$

where r_w is the inner radius of the chamber, ϕ is the

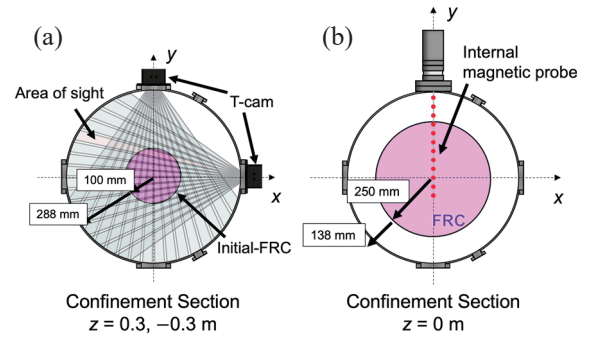


Fig. 3 (a) Cross sectional view of the FAT-CM device showing the line of sight direction of T-cam at two cross planes ($z = \pm 0.3$ m). (b) Cross sectional view of the FAT-CM device showing the location of the probe (marked with a red dot) in the center of the plane.

magnetic flux, and B is the magnetic field density. The subscripts “p” and “v” denote for the discharges with and without plasma, respectively. For the measurements in the confinement chamber, the confinement chamber can be considered flux-conserving tubes during the translational-collisional merging processes because the skin time (~ 5 ms) is much longer than the timescale of these processes so that $\phi_p = \phi_v$. Therefore, the excluded flux radius can be obtained with the measurement of B_v and B_p of the magnetic probe [7]. Two interferometers were installed on the midplane ($z = 0$ and -0.6 m) of the confinement section and one at the muzzle of the V-formation section ($z = 2.1$ m).

For observing the internal magnetic field profile of the FRC plasma, an internal magnetic probe array was installed on the midplane as shown in Fig. 3. To observe the radial motion during the translation process, an optical observation system for computed tomography (tomography camera: T-cam) [8] was installed in the confinement chamber (Fig. 3 (a)). The radial shift motion was estimated based on the radial distribution of bremsstrahlung radiation observed using the T-cams at two crossplanes ($z = \pm 0.3$ m) of the confinement section, as shown in Fig. 1. The time evolution of the particle inventory of a formed FRC was evaluated using He-Ne laser interferometers for measurement of the plasma density. A radial magnetic field profile was observed using the internal magnetic probe array [5].

3. Experimental Results

Figure 4 shows the typical behavior of FRCs in two cases with a small shift (case 1) and a larger shift (case 2). Figure 4 (a) shows the shift ($n = 1$) motion of the initial (before the collision) plasmoid measured using a T-cam. Each dot traces the center of gravity of the initial plasmoids at the time just before the collision. One of the simplest methods for estimating the center of gravity is to use the radial profiles of bremsstrahlung radiation observed using the T-cam. The interpolated profiles were integrated from

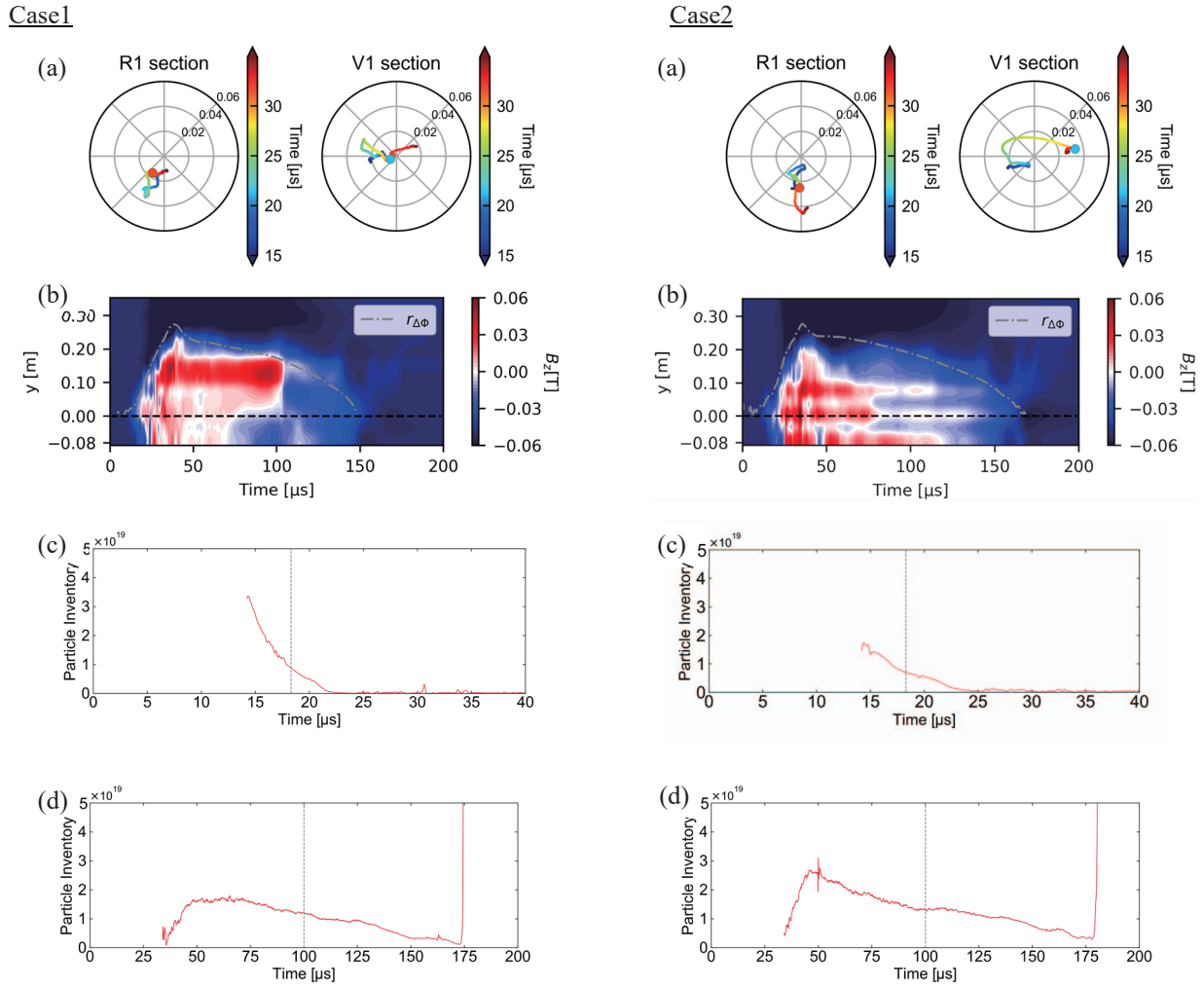


Fig. 4 Typical behavior of FRCs before and after the collision/merging process (Translational-collisional merging process: 20 - 40 μs , Relaxation process: 40 - 50 μs , Decay process: 50 - 200 μs). Time evolution of (a) the center of gravity of initial-plasmoid translation axes at the R1 section ($z = -0.3$ m) and V1 section ($z = 0.3$ m), (b) contour maps of magnetic fields (B_z) radial profiles, particle inventory at (c) the muzzle of the V-formation section and (d) the midplane in the confinement sections in each case. The dotted lines in (c) and (d) indicate the times of the observation.

the ends, and a channel with half of the total output value was determined as the center in each profile. The center of gravity was estimated by obtaining the intersection points of the determined center of each profile. Figure 4 (b) depicts the contour maps of radial magnetic field (B_z) profiles. The time evolution of the profile was obtained using the complementation of the measurement points of the magnetic probe [5]. Figures 4 (c) and 4 (d) show the time evolution of the particle inventory at the muzzle of the V-formation and the confinement sections, respectively. The length of FRC plasma is given by the full width of two-thirds of the maximum of the excluded flux radius axial profile at each time. The volume of the FRC plasma $V_{\Delta\phi}$ is given by the volume of the rotating body with the excluded flux radius $r_{\Delta\phi}$ inside the length of the FRC plasma. The average electron density \bar{n}_e was estimated by dividing the line-integrated electron density by the diameter of the plasma $2r_{\Delta\phi}$. Herein, the total particle inventory N can be calculated as follows: $N = \bar{n}_e V_{\Delta\phi}$. The particle loss

of FRC plasma before and after the collision can be estimated as the ratio of particle inventory at the midplane in the confinement section to twice that at the muzzle of the V-formation. Herein, the particle inventories in the V- and R-formations were assumed to be equal. In both cases, the field-reversed structure of the B_z profile was observed after the collision/merging even when there is a large difference in the offset.

Figure 5 depicts the dependence of the poloidal flux after merging on the offset at the collision. In the presented experiments, oppositely translated FRCs always have finite offset. Offset [%] is the ratio of the distance between the centers of gravity in the two cross sections to the excluded flux radius at the time of impact. Poloidal flux was estimated from the B_z radial profile measured using the internal magnetic probe array. Poloidal flux ϕ_p was defined as follows:

$$\phi_p = - \int_0^R 2\pi r B_z dr = \int_R^{r_{\Delta\phi}} 2\pi r B_z dr, \quad (2)$$

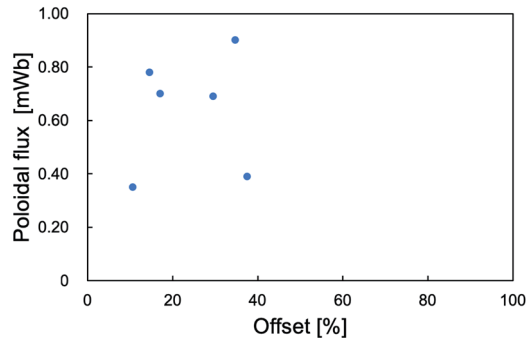


Fig. 5 Poloidal flux relative to offset before and after the collision.

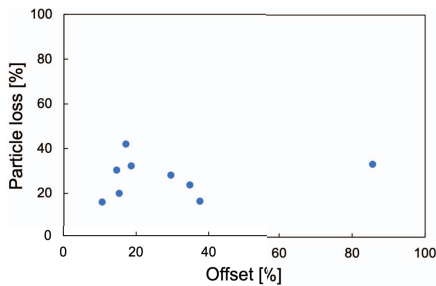


Fig. 6 Particle loss relative to offset before and after the collision.

where R is the radius of magnetic field neutral position ($B_z = 0$) [9]. Under a constant external magnetic field, the poloidal flux is approximately proposed to the cross sectional area of the plasma, as expressed in Eq. (2). In the presented experiments, there was no considerable dependence of the magnetic on the offset of the collision axes. The particle loss was almost the same, regardless of the offset of the collision axes. Figure 6 depicts the correlation between the offset of translation axes and the particle loss for several different plasma shots. In the presented experimental results, there is no considerable correlation between the offset of translation axes and the particle loss.

4. Prediction by 3D MHD Simulation Using the MIPS Code

Herein, considering both finite offset of the collision axis and any toroidal effects on the dynamics, we execute a MIPS simulation for predicting the 3D behavior of the merging. The FRC tends to be unstable to the tilt instability [10]. Figure 7 depicts 3D MHD simulation results for two different initial perturbations. At the beginning of the simulation, tiny perturbations less than 0.1% of the translational speed are added randomly to the velocity space. The first one is when initial perturbations of toroidal mode number $n = 1$, which gives the primary modeling of the observed offset, were applied to two FRCs before the collision, as shown in Fig. 7(b). The simulation result suggests that the radial displacement with $n = 1$ enhances tilt

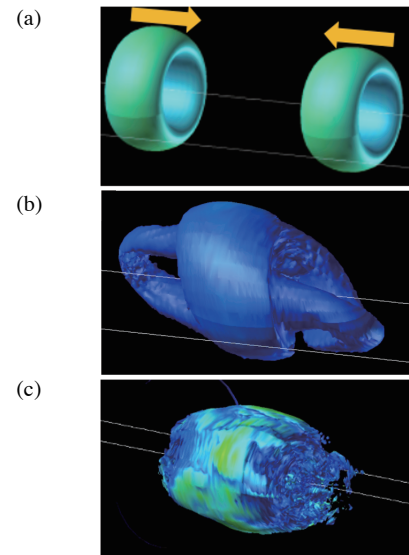


Fig. 7 3-D diagrams of the FRC plasma before and after the collision via 3D MHD simulation. (a) Two initial plasmoids before collision, (b) with initial perturbations of toroidal mode number $n = 1$ applied to both two FRCs, (c) with higher ($n < 8$) modes of initial perturbations.

instability. The second one is when initial perturbations with higher ($n < 8$) modes number were applied, as shown in Fig. 7(c). The simulation result suggests that applied initial perturbations with higher mode numbers suppressed tilt instability; however, the merged FRC collapses soon after the collision. The simulations predict that the FRC is not formed after the collisional merging process with the offset collisional axes without applying the initial perturbation. In the 3D MHD simulation, merging cannot be completed within a timeframe of the growth of the instabilities, even with modest perturbation.

5. Summary

During collision/merging processes, the initial FRCs have an even larger offset of collision axes and experience destructive perturbation during collision/merging processes. After merging, the FRC reaches a quiescent FRC equilibrium without considerable performance degradation in terms of particle inventory and trapped magnetic flux. By contrast, the 3D MHD simulation shows strong tilt and plasmoids merging is not completed, even with the modest initial disturbance of about 0.1% of the Alfvén speed. This difference between the experimental and simulation results suggests that the experimentally formed FRCs have an effective stabilization mechanism that maintains the axisymmetry of the dynamic merging process.

Acknowledgments

The authors would like to acknowledge all members of Fusion-Plasma group, Nihon University who contributed to discussion. This work was partially sup-

ported by JSPS KAKENHI Grant Number JP19K21868, JP20H00143, NIFS Collaborative Research Program Grant Number NIFS20KNST163 and Grants-in-Aid of College of Science and Technology, Nihon University.

- [1] M. Tuszewski, Nucl. Fusion **28**, 2033 (1988).
- [2] L.C. Steinhauer, Phys. Plasmas **18**, 070501 (2011).
- [3] T. Asai *et al.*, Nucl. Fusion **61**, 096032 (2021).
- [4] D. Kobayashi *et al.*, Phys. Plasmas **28**, 022101 (2021).
- [5] T. Watanabe *et al.*, Rev. Sci. Instrum. **92**, 053541 (2021).
- [6] Y. Todo *et al.*, Plasma Fusion Res. **5**, S2062 (2010).
- [7] M. Tuszewski *et al.*, Rev. Sci. Instrum. **54**, 1611 (1983).
- [8] H. Tomuro *et al.*, Rev. Sci. Instrum. **81**, 10E525 (2010).
- [9] H. Gota *et al.*, Rev. Sci. Instrum. **89**, 10J114 (2018).
- [10] R.A. Clemente and J.L. Milovich, Phys. Lett. **85A**, 148 (1981).